Particle Velocity Fluctuations in Steady State Sedimentation: Stratification Controlled Correlations.

P.N. Segrè and J.E. Davidheiser
Department of Physics, Emory University, Atlanta, GA 30322

The structure and dynamics of steady state sedimentation of semi-concentrated ($\phi = 0.10$) monodisperse spheres are studied in liquid fluidized beds. Laser turbidity and particle imaging methods are used to measure the particle velocity fluctuations and the steady state concentration profiles. Using a wide range of particle and system sizes, we find that the measured gradients $\nabla\phi$, the fluctuation magnitudes σ_v, and their spatial correlation lengths ξ, are not uniform in the columns - they all show strongly $z-$dependent profiles. These profiles also display a scaling in which results from different particle sizes collapse together when plotted in the forms $-a\nabla\phi(z)$, $\xi(z)/a$, and $\sigma_v(z)/v_p$, demonstrating the universality of the particle dynamics and structure in steady state sedimentation. Our results are also used to test a recently proposed model for the correlation lengths $\xi(z)$ in terms of the concentration stratification $\nabla\phi(z)$ [P.J. Mucha and M.P. Brenner, Phys. Fluids **15**, 1305 (2003)], $\xi(z) = c_0 a[\phi S(\phi)]^{1/5}[-a\nabla\phi(z)]^{-2/5}$. We find that the correlation lengths predicted by this model are in very good agreement with our measured values, showing that the origin of the fluctuation length ξ lies with the concentration stratification $\nabla\phi$.

PACS numbers: 47.15.Gf, 05.40.-a, 47.55.Kf, 82.70.Dd

I. INTRODUCTION

The slow sedimentation of a collection of non-Brownian spheres in liquids is a fundamental problem in physics and is of importance in numerous chemical industries[1]. Despite its apparent simplicity, the complexities of hydrodynamic interactions between particles are still vigorously debated[2,3,4,5,6]. Much of the debate surrounds the origin of the characteristic size of velocity fluctuations, $\xi \sim 11a\phi^{-1/3}$, found in sedimentation experiments[7,8] (Here a is the particle radius and ϕ is the volume fraction). This lengthscale is typically smaller than the cell dimensions and plays a central role in sedimentation dynamics. The magnitude of the particle velocity fluctuations σ_v depends directly on ξ. In dilute suspensions, Poisson statistics dictates that in a region of size ξ, the typical concentration fluctuation is $\sigma_\phi = \sqrt{\phi a^3/\xi^3}$; its velocity is determined by balancing its buoyant weight, $\sigma_\phi \Delta\rho g \xi^3$, with its Stokes drag, $6\pi\eta\xi\sigma_v$, giving $\sigma_v \propto \sqrt{\phi\xi/a}$.[7,9] Similarly, particle diffusion coefficients, $D \sim \xi\sigma_v$, also depend directly on ξ.[8] Due to its central role, an understanding of the origin of the fluctuation correlation length is essential for even a basic description of sedimentation.

Recent theories[10,11,12,13,14] have taken a new approach to understanding the lengthscale of velocity fluctuations by considering the possible effects of a small stratification in mean column concentration, $\nabla\phi$. Mucha and Brenner[12,13] argue that because velocity fluctuations of size l are driven by buoyancy forces acting on local concentration fluctuations σ_ϕ, when there is a concentration variation across the fluctuating region due to the stratification $l\nabla\phi$ that is of order the fluctuation itself, $\sigma_\phi = \sqrt{\phi a^3/l^3}$, then the buoyancy mismatch of the fluctuating region is reduced, and motions are suppressed. The largest region for which motion occurs then is of order $l = -\sigma_\phi/\nabla\phi$, or

$$l/a = c_0[\phi S(\phi)]^{1/5}[-a\nabla\phi]^{-2/5}, \qquad (1)$$

which relates the correlation size l to the concentration stratification $\nabla\phi$. Here, the static structure factor $S(\phi)$ accounts for excluded volume affects in non-dilute samples[8]. Results in support of this model[12], using numerical simulations, have focussed on the diffusion coefficients at the transition region near the top particle interface. The generality of the Mucha and Brenner (MB) model, however, suggests it is not confined solely to interfacial properties, and may provide a complete description for the fundamental length ξ over the entire sedimenting column.

The most direct test of the MB model, as performed in this article, would be a direct comparison between measured fluctuation lengths ξ, and the calculated stratification lengths l, over all heights in a sedimenting particle column. This test has yet to be done, principally due to a lack of data for both $\xi(z)$ and $\nabla\phi(z)$. Moreover, the few available data for $\nabla\phi$ far from the interface, using simulations, yield seemingly contradictory results; Ladd[15] found negligibly small gradients, but Mucha and Brenner[12] found much larger ones. We note that since Mucha and Brenner considered larger systems than Ladd, this contradiction may be resolved if gradients have an as yet unidentified system size dependency.

In this article we examine steady state sedimentation using a wide range of particle and system sizes. The samples have the same column height, H, and the same mean concentration, $\phi_0 = 10.0\%$, but different particle sizes a, which range over a factor of ~ 4.5 so that the system size N ($\propto a^3$) varies by almost two orders of magnitude. We first show that all of the samples show some degree of stratification. The magnitude of the stratification increases with (normalized) cell size until its average becomes of order $\overline{\nabla\phi} \sim \phi_0/H$. We then show that

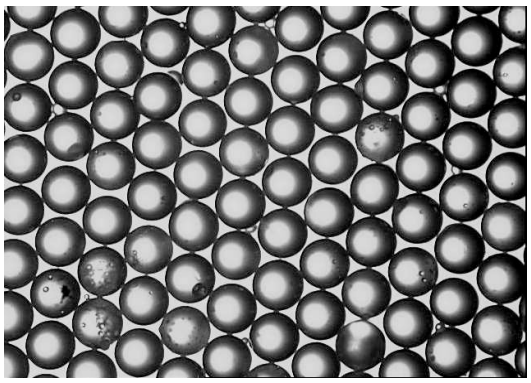

FIG. 1: Photograph of a random sampling of $a = 154.5$ μm spheres resting on a glass slide.

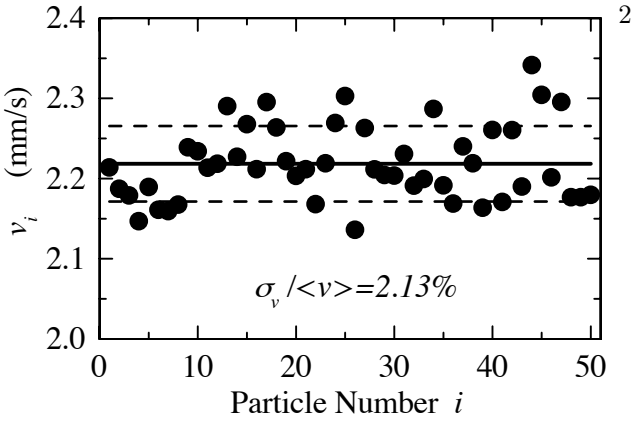

FIG. 2: The settling velocities of 50 isolated spheres falling in a water/glycerol mixture. The solid line is the average settling rate, $v = 2.218$ mm/s, and the dashed lines the standard deviation, $\sigma_v = 0.047$ mm/s. The polydispersity in velocity is $\sigma_v/v = 2.13\%$, corresponding to a particle size polydispersity of $\sigma_a/a = 1.07\%$.

there is a scaling regime in which the (height-dependent) concentration gradients, the velocity correlation lengths, and the velocity fluctuation magnitudes all collapse onto master curves when scaled as $-a\nabla\phi(z)$, $\xi(z)/a$, and $\sigma_v(z)/v_p$. All of our data are consistent with the MB model. We find that the stratification lengths $l(z)$ calculated from Eq. (1) agree with our measured values $\xi(z)$ using a single fit constant, $c_0 = 0.82$, for three different samples in the scaling regime, and a slightly lower value, $c_0 = 0.70$, in the non-scaling regime. These findings validate the physical picture behind the MB model, and show that the origin of the fluctuation length ξ lies with the concentration stratification $\nabla\phi$.

Our choice of an experimental arrangement to study $\nabla\phi$ is guided by the recent observations of persistently evolving gradients during sedimentation[10,16,17]. The evolution occurs because, starting from a well mixed sample ($\nabla\phi = 0$), it takes some time for the stratification ($\nabla\phi \neq 0$) to become established. During this evolution, the column is falling, and often steady state is never reached before all the particles lie on the bottom[10]. To ensure we reach a steady state, we conduct experiments in a fluidized bed apparatus, where liquid is pumped upwards to balance the settling of the particles[18,19]. The flow balancing ensures that the particle column never collapses, and a steady state is eventually established.

II. EXPERIMENT DESCRIPTION

A. Particles and Fluids

We use spherical glass beads of mean radii $a = 54.5, 103.5, 154.5$, and 245 μm. The beads have been specially filtered by the manufacturer (Mo-Sci corp.) to be of extremely low polydispersity in size. To demonstrate this, we show in Fig. 1 a micrograph of a collection of the $a = 154.5$ μm beads. The particles lay on a flat plate and through a gentle shaking quickly organize into highly ordered forms, indicative of low levels of polydispersity σ_a. To accurately determine σ_a, for each set of particles we measure the variation in settling velocities of 50 individual spheres. Fig. 2 shows the results for the $a = 245$ μm spheres. The standard deviation of the individual particle settling rates is indeed extremely low, $\sigma_v/v = 2.13\%$. Using the Stokes formula[1], $v_0 = (2/9)\Delta\rho g a^2/\eta$, and assuming the particles are all of equal density, the variation in settling rates correspond to a variation in particle size of $\sigma_a/a = 1.07$ %. This procedure is repeated for all 4 particle sizes, with the results listed in Table I. In all cases, the measured value of the size polydispersity σ_a/a is less than 1.7%.

TABLE I: Particle, fluid, and fluidized bed properties. a is the average particle radius, σ_a/a the measured size polydispersity, η the pure solvent viscosity, v_0 the Stokes settling velocity, Re the particle Reynolds number, H the total height of the fluidized particle column, and ϕ_0 the average volume fraction of the fluidized bed.

$a(\mu m)$	σ_a/a	η (cp)	$v_0(mm/s)$	Re	H (cm)	ϕ_0
54.5	0.016	17	0.548	0.002	18.5	0.10
103.5	0.015	27	1.21	0.005	18.5	0.10
154.5	0.012	54	1.34	0.004	18.5	0.10
245	0.011	87	2.10	0.006	18.5	0.10

The glass beads are dispersed in viscous solutions of glycerol and water chosen so that inertial forces during fluidization are negligible. The particle Reynolds numbers, listed in Table I, are all of order $Re = v_0 a\rho/\eta \approx 5 \times 10^{-3} \ll 1$. Additionally, particle motions always occur at very high Peclet numbers ($Pe \approx 10^9$), so that Brownian diffusion is negligible. The temperature is at the ambient value $T = 21^o$C.

FIG. 3: Photographs of a fluidized particle bed comprised of $D = 490$ μm spheres. LHS - whole cell. RHS - closeup of the top of the column.

B. Fluidized Bed

The fluidized bed, shown in Fig. 3, consists of a fluid and particle filled glass cell at the bottom of which fluid is pumped upwards to counteract the particle settling and *fluidize* the particles. The sample cell is a rectangular glass tube of dimensions $T \times W \times H = 8 \times 80 \times 305$ mm. The overflow liquid at the top of the cell recirculates back into the pump, forming a closed loop. To enable a uniform flow into the cell, a 2 cm thick nylon mesh is packed with 0.5 mm diameter beads and glued across the entrance to the cell at the bottom.

In the experiments described below, we use this setup to fluidize four different particle size samples, as listed in Table I. To examine the specific effects of particle size, all four samples share the same average particle concentration, $\phi_0 = 0.10$, and same total height of the particle column H. With the pump off, the spheres in all 4 samples form a sediment at the bottom ~ 2.9 cm tall. When the pump is on, the particles expand upward, filling a region above the bottom up to a height dependent upon the pumped fluid velocity v_p (see Fig. 3). For all 4 samples, we set v_p to a value that expands the particle column to a total height $H \sim 18.5$ cm, so that the average volume fraction is approximately the same for all of the samples, $\phi_0 = \phi_{RCP} * (2.9/18.5) \sim 0.10$, where $\phi_{RCP} = 0.638$ is the assumed value for the sediment at the random close packing density.

C. PIV Imaging System: Velocity Flow Maps

Particle velocities are measured using the technique of particle image velocimetry (PIV)[20]. The apparatus consists of a (1008 × 1024 pixels) CCD camera, a synchronized stroboscope illuminating the cell from behind, and specialized image processing hardware and software from Dantec Instruments. The depth of field of the camera lens is ≈ 5 mm. A large cross section of the cell is imaged so that several thousand particles can be simultaneously studied. Velocity maps consisting of 62 × 62 vectors are extracted by comparing two closely timed pictures using standard PIV techniques. Each vector is the average velocity of two to four spheres.

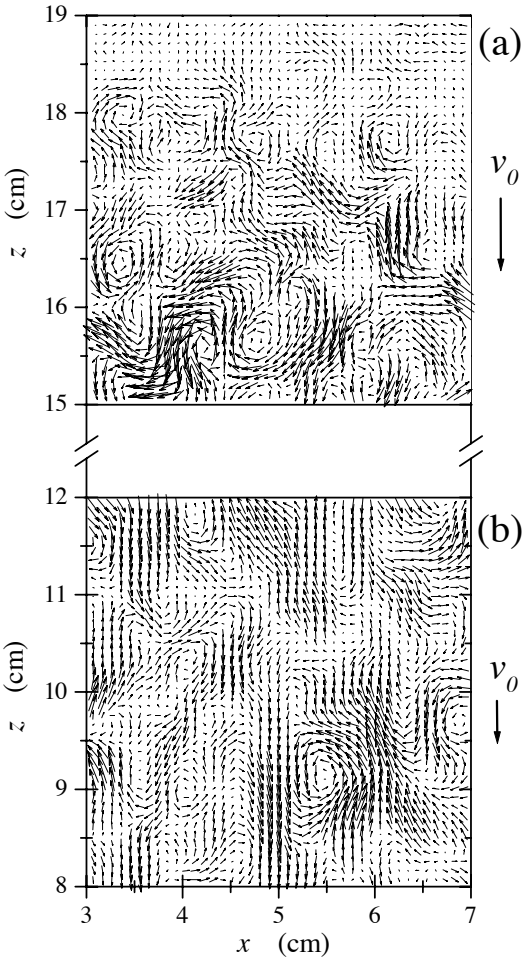

FIG. 4: Velocity vector maps of a stable fluidized bed of average concentration $\phi_0 = 0.100$. Figures 1 (a) and (b) correspond to respective positions near to the top and near to the middle of the particle column. The single arrow on the right gives the corresponding scale of the Stokes settling velocity v_0. Note that the velocity scale in (a) is magnified relative to (b) by a factor of 2 for clarity.

Figure 4 shows typical velocity vector maps from a stable fluidized bed, where (a) corresponds to a position near the top and (b) to a position near the middle of the particle column. For scale, we also show the magnitude of the Stokes settling velocity v_0. Both velocity maps show regions moving upwards and downwards, and, as in all of our samples, the magnitudes of the velocities are significantly larger near the middle than near the top.

To quantify these observations, we measure the velocity maps at different heights z along the particle column. We extract from the velocity maps the mean velocities, $\overline{v}_z = \langle v_{i,z} \rangle$, and the root mean square (rms) velocity fluctuations, $\sigma_v^z = \langle (v_{i,z} - \overline{v}_z)^2 \rangle^{1/2}$, where $\langle \ldots \rangle$ represents an ensemble average over ~ 50 vector maps of

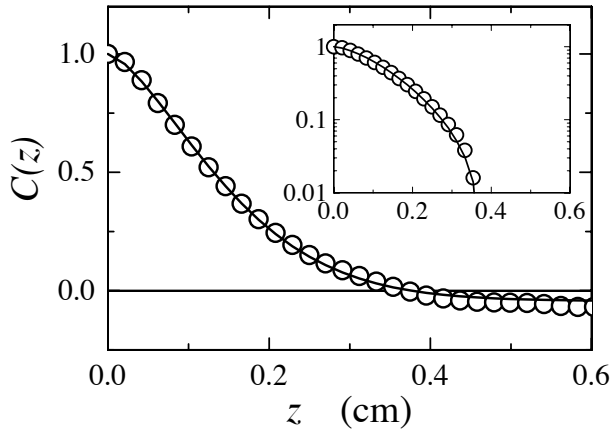

FIG. 5: Correlation functions of the velocity fluctuations $C(z)$ as a function of distance z, near mid-height in the $a = 54.5$ μm particle fluidized bed. The inset shows the logarithm of $C(z)$, the solid line being a fit to $C(z) = \exp(-(z/\xi)^{1.5})$, from which we extract values of the correlation lengths ξ.

3844 vectors each.

The typical velocity vector maps in Fig. 4 also display large regions where the velocity vectors are spatially correlated. To quantify this, we calculate the normalized spatial correlation functions of the vertical velocity v_z, defined as $C(z) = \langle v_z(0)v_z(z)\rangle / \langle v_z(0)^2\rangle$. Figure 5 shows typical results for $C(z)$, measured near mid-height in a fluidized bed of $a = 54.5$ μm particles. The inset shows that the empirical form $C(z) = \exp\left(-(z/\xi)^{1.5}\right)$ fits the data well, enabling us to extract values for ξ, the characteristic (vertical) correlation length of the velocity fluctuations.

1. *Fluidized Bed Stability*

Before using the fluidized bed apparatus for data collection we need to ensure that the bed is stable in time and that there are no large scale convective currents indicative of an unbalanced (i.e. tilted) cell. To do this we use the PIV imaging method and examine particle velocities over different regions in the cell. Figure 6 shows typical results for $\overline{v}$ and σ_v, both perpendicular and parallel to gravity, from PIV vector maps spanning a 4×4 cm imaging window near mid-height. All quantities randomly fluctuate, but they also maintain time-invariant mean values indicative of a stable system. Additionally, both velocity averages fluctuate about $\overline{v} = 0$, explicitly demonstrating that particle sedimentation downwards is balanced by the fluidizing counter flow upwards. During the experiments, we monitor the mean velocities to ensure stability, and we also record the position of the top particle/fluid interface, clearly visible in Fig. 3, to ensure that it does not rise or fall in the cell over time.

As a way of further demonstrating the stability of the bed, we apply an uncontrolled shock to the system

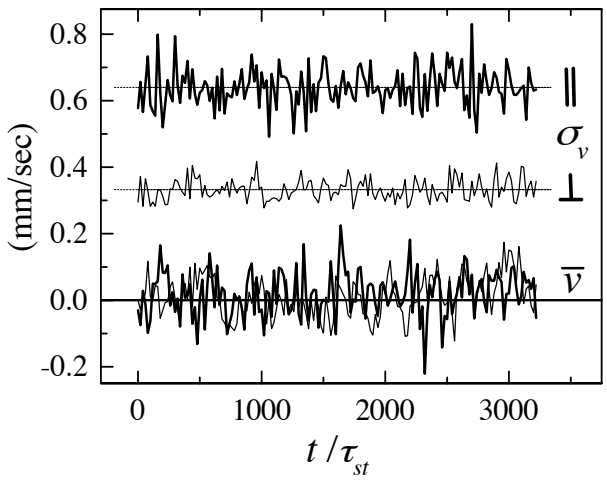

FIG. 6: Fluidized bed stability: Average velocities $\overline{v}$, and velocity fluctuations σ_v, parallel (thick lines) and perpendicular (thin lines) to gravity as a function of time t/τ_{st}, where $\tau_{st} = a/v_0$ is the Stokes time. The imaging window is near mid-height in a fluidized bed of particles of mean size $a = 154.5$ μm.

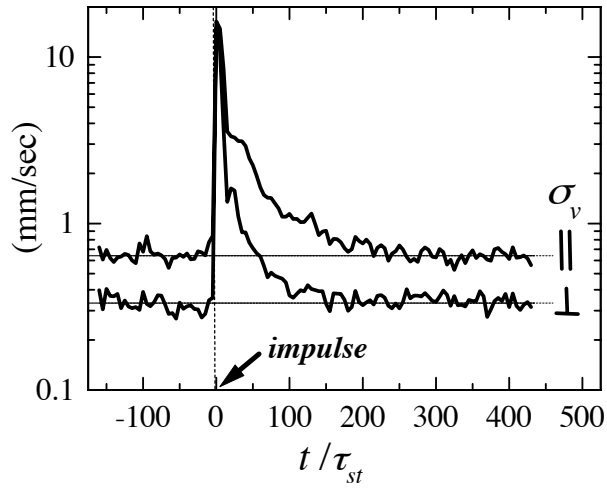

FIG. 7: Response of a stable fluidized state to a large perturbation. The velocity fluctuations σ_v, both parallel and perpendicular to gravity, as a function of time t/τ_{st}. At time $t = 0$ a rapid and large scale impulse is applied throughout the particle bed to disrupt the particles.

and examine whether or not it returns back to its original state. Figure 7 shows the test results in which we inject a large (~ 3 cm radius) air bubble into the middle of the particle bed to cause a rapid and large scale disruption to the particles. The particle velocity fluctuations σ_v, from a 4×4 cm subsection of the cell at mid-height, are driven to values at $t = 0$ that are more than 10 times their values before the shock. Nevertheless, this disturbance rapidly decays away until, for times $t \gtrsim 250\tau_{st}$, the system returns to its prior stable state.

D. Light Scattering System; Particle Concentrations.

Local particle volume fractions are determined from the local optical turbidity through the particle column. We pass an expanded He-Ne laser beam, of diameter ~ 0.5 cm, through the fluidized bed at a particular height z, and measure the transmitted laser intensity $I_T(z)$ using a CCD camera. Results for a typical sample are shown in Fig. 8. Figure 8(a) shows the measured intensity profiles on the CCD at different heights in the particle column. It's evident that the transmitted intensity varies with height, with the highest intensity at the top, and the lowest at the bottom. To find the corresponding particle concentrations, we need a calibration reference for the dependence of the transmitted intensity on particle concentration. To do this, we make several reference fluidized beds of differing average concentration ϕ and measure the transmitted intensity patterns at mid-height. The concentration values are calculated from the ratio of the heights of the sedimented particles, at H_{sed} and $\phi = 0.638$, to the height of the fluidized column, H, as $\phi = 0.638 * (H_{sed}/H)$. The results are shown in Fig. 8(b). No efforts are made to model the observed dependence of I on ϕ, our aim being simply to have a calibration reference. Fits of $I(z)$ and $I(\phi)$ in Fig. 8(a) and (b) to Gaussian functions yield peak intensity values I_{pk}, plotted in Fig. 8(c). By comparing the measured values of $I_{pk}(z)$ in our fluidized bed with the reference values of $I_{pk}(\phi)$ we are able to determine the height dependent concentrations $\phi(z)$ in the fluidized beds, as shown in Fig. 8(d).

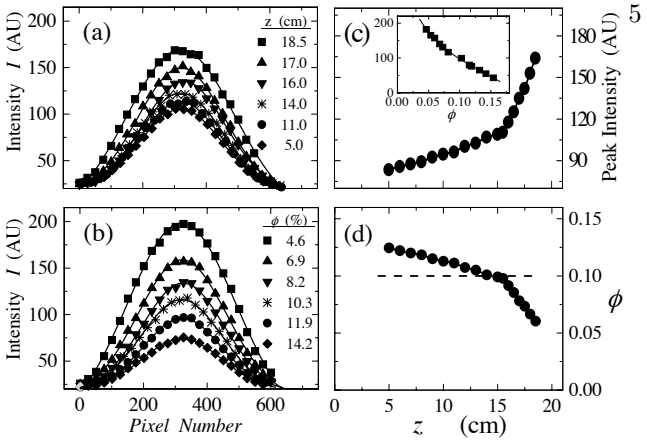

FIG. 8: (a) Transmitted laser intensity I vs. height z through a fluidized bed of radii $a = 103.5$ nm particles at average volume fraction $\phi_0 = 0.10$. The solid lines are fits to Gaussian functions. (b) Intensity vs. ϕ calibration. Transmitted laser intensities measured at mid-height in fluidized beds of average volume fraction $0.046 \leq \langle\phi\rangle \leq 0.142$ as labelled. For clarity, only every 25'th point is plotted. The solid lines are fits to Gaussian functions. (c) Peak transmitted intensity $I_{pk}(z)$ vs. height z as extracted from Gaussian fits to the data in (a). Inset: Calibration curve of peak transmitted intensity $I_{pk}(\phi)$ vs. ϕ as extracted from Gaussian fits to the data in part (b). (d) Volume fraction ϕ vs. height z as determined by comparing the $I(z)$ curve in (c) with the calibration curve $I(\phi)$ in the inset of (c).

III. RESULTS

In this section we describe our main results for the particle dynamics of 4 fluidized beds that all share the same average particle concentration, $\phi_0 = 0.10$, and column height, $H = 18.5$ cm. The beds differ, however, in the size of the fluidized particles, which range from $54.5 \leq a \leq 245$ μm. As a consequence, the beds differ in two significant ways. First, the normalized bed heights, $H^* \equiv H/a$, range from 755 for the largest particles to 3364 for the smallest. Second, the total number of particles fluidized, $N = [(3/4\pi)\phi_0 TWH] \times a^{-3}$, range from $192,000 \leq N \leq 17,500,000$, as listed in Table II. A comparison of the results for different particle sizes will allow us to examine the specific dependencies of fluidization on the system size N, and the effective column height H^*. For each fluidized bed we present results for the height dependence of the particle concentration $\phi(z)$, the velocity fluctuations $\sigma_v(z)$, and the velocity correlation lengths $\xi(z)$.

TABLE II: Measured properties of the fluidized beds described in Table I. a is the particle radius and N the total number of particles fluidized. v_p/v_o is the normalized fluidizing pump velocity upwards. v^{top}/v_o is the initial sedimentation velocity of the top interface, measured just after the fluid pump is turned off. ϕ^{top} is the particle concentration measured just below the top interface. The particle concentrations ϕ_p^{top} and ϕ_{sed}^{top} are calculated from v_p/v_o and v_{sed}^{top}/v_o using the Richardson-Zaki equation $v/v_o = (1-\phi)^{5.5}$.

$a(\mu m)$	H^*	N	$\frac{-v_{sed}^{top}}{v_o}$	$\frac{v_p}{v_o}$	ϕ^{top}	ϕ_{sed}^{top}	ϕ_p
245	755	$1.92 \cdot 10^5$	0.605	0.600	8.4 %	8.7 %	8.9 %
154.5	1194	$7.67 \cdot 10^5$	0.659	0.654	7.0	7.3	7.4
103.5	1769	$2.55 \cdot 10^6$	0.727	0.686	6.0	5.6	6.6
54.5	3364	$1.75 \cdot 10^7$	0.797	0.776	3.7	4.0 %	4.5

A. Concentration Profiles $\phi(z)$.

We begin by examining the concentration profiles $\phi(z)$ of the four different particle size fluidized beds. The laser scattering method, described in section II.D above, allows for the accurate determination of the local particle volume fraction $\phi(z)$ as a function of height z. To do this, we first fluidize each of the four different particle sized samples to the same mean concentration, $\phi_0 = 0.100$, and the same total height, $H = 18.5$ cm. After waiting for transients to die out (a time $> H/v_0 \sim 5$ min) we obtain the time invariant concentration profiles shown in

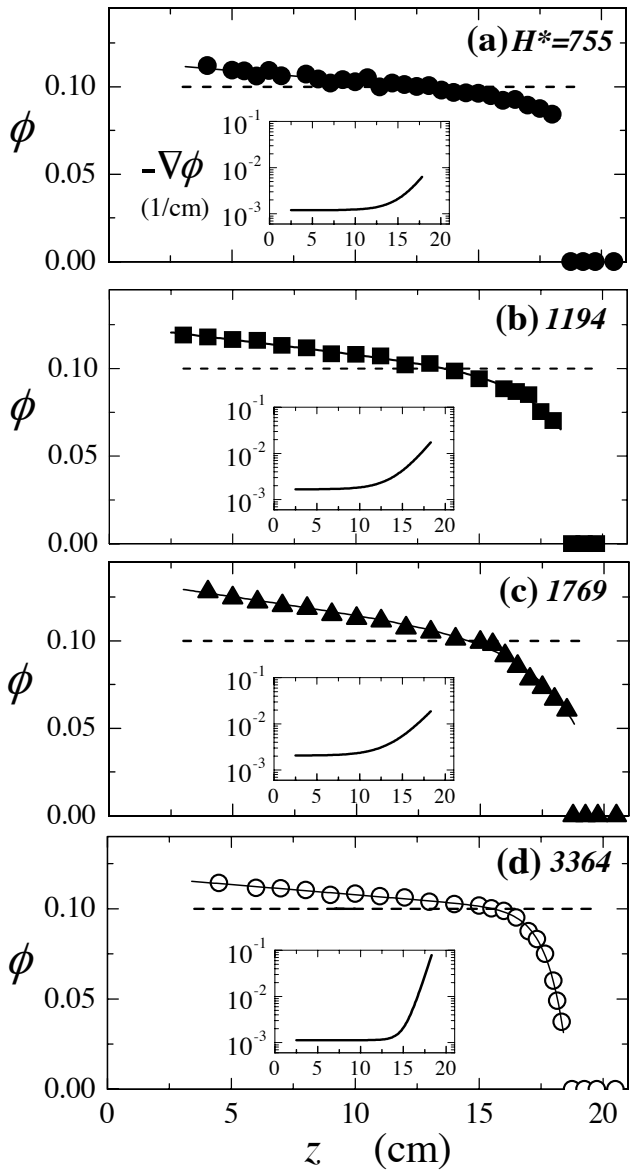

FIG. 9: Steady state concentration profiles $\phi(z)$. The particle radii, normalized column height, and number of particles are (a) $a = 245$ μm, $H^* = 755$, $N = 1.92E5$, (b) $154.5, 1194, 7.67E5$, (c) $103.5, 1769, 2.55E6$, and (d) $54.5, 3364, 1.75E7$. The dashed lines show the mean concentrations, $\phi_0 = 0.100$. Solid lines are fits to the empirical form $\phi(z) = b_0 - b_1 z - b_2 e^{b_3 z}$, where b_0, b_1, b_2 and b_3 are adjustable fit constants. Insets: concentration gradients, $-\nabla\phi = b_1 + (b_2 b_3) e^{b_3 z}$.

Figs. 9(a-d).

It is immediately apparent that none of the fluidized beds are perfectly homogeneous in concentration. Each concentration profile shows the same trend for the concentration to decrease with height, i.e. they are all stratified. While most of the concentration variation occurs in the highest portions of the columns, measurable and significant gradients occur at all heights.

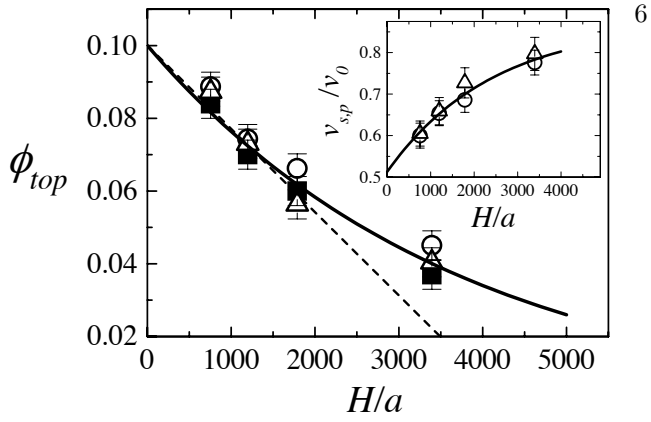

FIG. 10: The concentration just below the top interface ϕ^{top}, $\circ$, vs. normalized column height H^*, from Fig. 9. Also shown are the volume fractions ϕ calculated from measurements of the settling velocities of the top interface, v_{sed}^{top}, $\blacksquare$, and the fluidization pump velocity v_p/v_0, $\triangle$, using the RZ equation $v(\phi)/v_0 = -(1-\phi)^{5.5}$. Inset: The initial settling velocity of the top interface, $-v_{sed}^{top}$, $\blacksquare$, and the fluidization pump velocity v_p/v_0, $\triangle$, as a function of column height H^*.

Perhaps the most striking result in Fig. 9 is that the concentration profiles and the degree of stratification change with normalized bed height $H^* \equiv H/a$. That is, despite the fact that all of the fluidized beds share the same average concentration, $\phi_0 = 0.100$, and the same total height $H = 18.5$ cm, there is no universal curve for the concentration profiles. Rather, the profiles are found to markedly change with normalized height H^*. The main trend in evidence, as described further below, is for the degree of stratification to increase with increasing cell height H^*, or system size N.

1. *Interfacial Concentrations.*

Before examining the details of the gradients in concentration $\nabla\phi(z)$ from Fig. 9, we first find it instructive to consider a simpler measure of the degree of nonuniformity in the beds by considering a measure of the variation of $\phi(z)$ in each column. The smallest values of $\phi(z)$ are always recorded at the tops of each column, just below the sharp interfaces (see Fig. 3 and 11). To within our resolution of ~ 0.5 cm, there is a near discontinuity as the concentration drops from a finite value to zero over ~ 0.5 cm. (Note that much more diffuse interfaces occur for more dilute and/or polydisperse systems[18,19,21]). We therefore define ϕ^{top} as the value of $\phi(z)$ measured closest to, and just below, the top interface.

Figure 10 shows our measured values of ϕ^{top} vs. the normalized bed height H^*. The overall trend is clear, the taller the column H^*, the smaller the concentration ϕ^{top}, and the greater the degree of stratification. For our 3 shortest columns, there is a near linear decrease of ϕ^{top} with H^*. This linear trend, of course, cannot continue

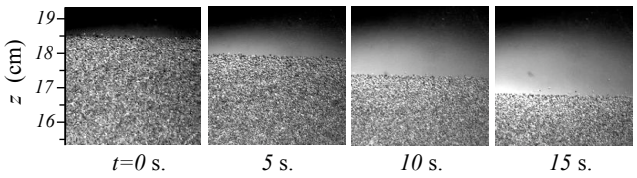

FIG. 11: Photographs of the top portion of a particle column, comprised of $a = 154.5$ μm spheres, taken at different time intervals t *after* having turned off the fluidizing pump.

indefinitely, as ϕ^{top} cannot go below zero. Indeed, in our tallest bed, the result deviates significantly from the initial linear trend.

To help corroborate the concentration values ϕ^{top} just below the top interface, we also conduct a second series of measurements. Because the hindered settling function of a collection of spheres is strongly ϕ-dependent (the Richardson-Zaki (RZ) equation[22] is $v(\phi)/v_0 = (1-\phi)^{5.5}$), by measuring the settling velocity of the top interface, v_{sed}^{top}/v_0, we can independently extract out values for ϕ^{top}. To test this, we first establish a stable fluidized bed, then turn off the fluidizing pump and measure the initial settling rate of the top interface, $-v_{sed}^{top}/v_0$. Figure 11 illustrates how these experiments are done. Results for $-v_{sed}^{top}/v_0$ vs. H^* are shown in the inset of Fig. 10. The corresponding (RZ calculated) values of ϕ^{top} are shown in the main portion of the Figure, and agree to within the error bars with the turbidity measurements. In this way, we have a second, independent, way of determining ϕ^{top} that further corroborates the non-universality of the concentration profiles with particle size a.

B. Concentration Gradients $\nabla\phi(z)$.

The insets in Fig. 9(a-d) show the concentration gradients $-\nabla\phi$, as derived from fits to $\phi(z)$. The gradients are all nearly constant up to mid-height, and increase markedly thereafter. They also increase in magnitude with decreasing particle size a. To examine this in closer detail, we plot in Fig. 12 the scaled values $-a\nabla\phi$ vs. height z. Remarkably, data for the 3 largest particle sizes collapse closely together, showing that in this regime there is a new scaling relation, $-\nabla\phi \propto 1/a$. This scaling also shows that the stratification increases with system size. Since the total number of particles in our samples, $N \propto 1/a^3$, we can equivalently recast the scaling form as $-\nabla\phi \propto N^{1/3}$. Significantly, this form predicts that in limit of small system sizes, $N \to 0$, the stratification vanishes so that the sample becomes homogeneous in concentration.

It is also readily apparent that the scaling form $-\nabla\phi \propto 1/a$ predicts an un-physical divergence of $-\nabla\phi$ in the small particle limit $a \to 0$. Consequently, the scaling form $-a\nabla\phi$ must eventually break down for small enough particles, and indeed, we do see large a large deviation from scaling in Fig. 12 for our smallest particle

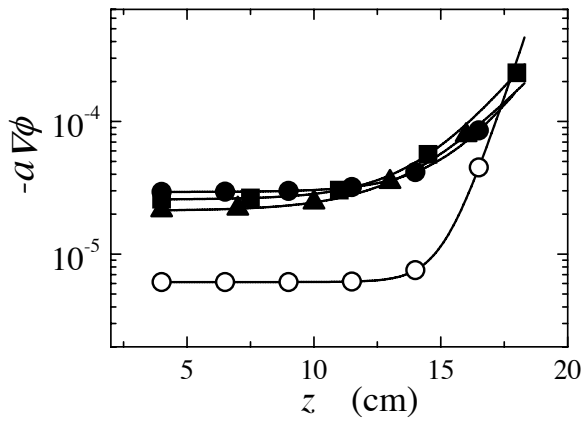

FIG. 12: Scaling of the concentration gradients, $-a\nabla\phi$ vs. height z, from fits to the $\phi(z)$ profiles shown in Fig. 9 ($-a\nabla\phi = ab_1 + (ab_2b_3)e^{b_3 z}$). The smallest particle size deviates from scaling because the gradient cannot exceed its maximum value (see text). The different symbol shapes correspond to differing particle sizes as defined in Fig. 9.

size, $a = 54.5$ μm. To help explain this, we note that the largest (linearly averaged over all heights z) value of $-\nabla\phi$ that is physically possible, for a bed of height H and average concentration ϕ_0, is $\langle -\nabla\phi \rangle_{max} \sim 2\phi_0/H$. Our height averaged gradients in the scaling regime, $-\langle \nabla\phi(z) \rangle \equiv \frac{1}{H}\int_0^H \nabla\phi(z)dz \sim 4.6 \cdot 10^{-5}/a$, will reach this maximum gradient when the particles become small enough, of order $a^* \sim 4.6 \cdot 10^{-5} H/2\phi_0 \sim 43$ μm. By these arguments, the $-a\nabla\phi$ data collapse cannot be maintained for bead sizes $a \lesssim a^* = 43$ μm, because this would require $\langle -\nabla\phi \rangle$ to exceed its maximum value $2\phi_0/H$. Consequently, for beads close to or smaller than a^*, plots of the product $-a\nabla\phi$ should deviate below those seen in the scaling regime, exactly as we see in Fig. 12 for our only set of beads that are close in size to a^*.

1. *Stratification Prediction Resulting from Particle Size Polydispersity*

Before continuing further, we critically examine the degree to which our results for $\nabla\phi(z)$ may be influenced by the non-zero particle size polydispersity σ_a/a of our beads. In general, a concentration stratification can arise due to a combination of (1) an inherent physical process found in monodisperse beads, and (2) purely the effects of particle size polydispersity. Several relevant points can be made for our systems. Firstly, we note that all 4 particle sizes used have similar levels of polydispersity, with $1.1 \leq \sigma_a/a \leq 1.6\%$, yet the degree of stratification varies greatly between the samples, suggesting that polydispersity is not the root cause. Additionally, recent computer simulations[23] compared the sedimentation dynamics and structure of particles with polydispersities ranging from 0% (perfectly monodisperse) up to 10%. While differences between the monodisperse and 10%

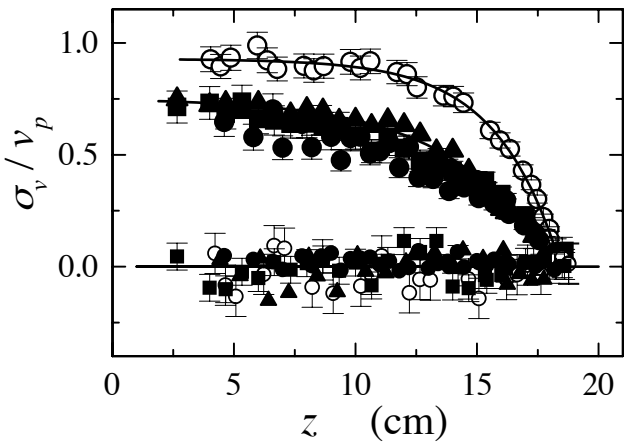

FIG. 13: Normalized velocity fluctuations σ_v, large symbols, and the mean particle velocity $\overline{v}$, small symbols, parallel to gravity as a function of height z in stable fluidized beds. The different symbols correspond to the different particle sizes as defined in Fig. 9. The solid lines are guides to the eye.

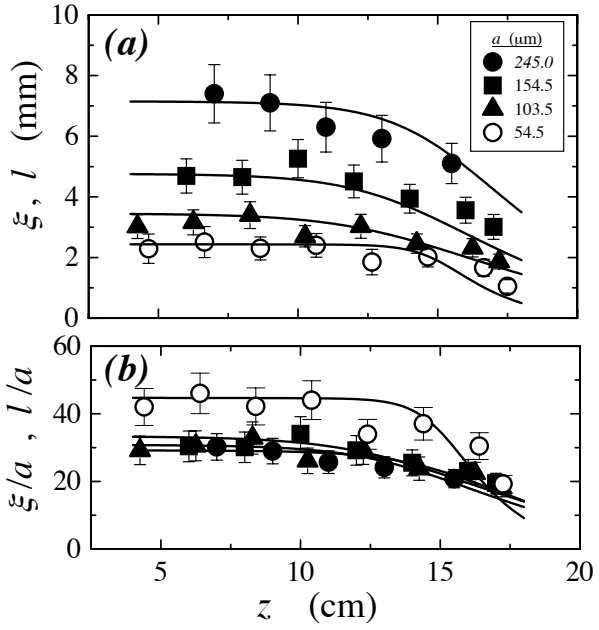

FIG. 14: Velocity correlation lengths plotted as ξ vs. height z in (a), and ξ/a in (b). The solid lines in (a) are the predictions of MB model for l, Eq. (1), with fit constants, in order of decreasing particle size, $c_0 = 0.82, 0.82, 0.82$ and 0.70. (b) The MB predictions for l/a.

cases were found, a polydispersity of 2%, slightly larger than our samples, yielded results that were, to within errors, identical to the monodisperse case. These arguments suggest that particle size polydispersity is not the dominant cause of the observed concentration gradients.

C. Velocity Fluctuations σ_v.

To measure the particle velocity fields, we use PIV methods. Figure 13 displays the values of the particle velocities for the 4 different particle size fluidized beds. Measurements are taken at multiple heights from near to the bottom up to the top, at a height of $H \sim 18.5$ cm. In all 4 samples the average velocities $\overline{v} \sim 0$, indicative of stable fluidization. Results are also shown for the normalized velocity fluctuations, σ_v/v_p, for the four different particle size beds.

In all samples, the fluctuation amplitudes decrease with height z in the column. At the top, fluctuations become vanishingly small, i.e. the particles are barely moving, which we also confirm by direct observation.

The behavior of the velocity fluctuations also mirrors that of the concentration gradients. That is, as found for $-a\nabla\phi$ in Fig. 12, Fig. 13 shows (i) a scaling regime, for $a \gg a^*$, in which the fluctuation values $\sigma_v(z)/v_p$ collapse together, and (ii) deviations from scaling for $a \sim a^*$.

D. Velocity Fields-Correlation Lengths

We next describe the characteristic lengthscale ξ of the velocity flucutuations. From the velocity maps as measured by PIV, we calculate the spatial correlation functions[7] of the vertical velocity fluctuations, $C(z) = \langle v_z(0)v_z(z)\rangle/\langle v_z(0)^2\rangle$, fit them to the form $C(z) = \exp\left[(-z/\xi)^{1.5}\right]$, and extract values for for ξ for the 4 different particle size fluidized beds are shown in Fig. 14(a).

The correlation lengths are not uniform in height, and exhibit a slight decrease towards the top part of the column[19]. Moreover, at every height z, ξ increases in magnitude with increasing particle size. To examine this further, we plot in Fig. 14(b) the values of the correlation lengths normalized by their particle radii, i.e. ξ/a. Significantly, the correlation lengths show the same behavior as the concentration gradients and fluctuation magnitudes. That is, (i) a scaling regime, for $a \gg a^*$, in which the correlation lengths $\xi(z)/a$ collapse together, and (ii) deviations from scaling for $a \sim a^*$.

E. Connections between Fluidization and Sedimentation

While in this article we focus entirely on the dynamical properties of fluidized particle beds, it is also of interest to understand the similarities between fluidization and sedimentation. In the lab frame, fluidization and sedimentation differ in that fluid is pumped upwards in the former, and not pumped at all in the latter. In the particle frame of reference, however, the particles in both cases are moving through a background fluid at a rate determined by their buoyant mass and concentration. It is not evident, *a priori*, how the particle dynamics differ between fluidization and sedimentation.

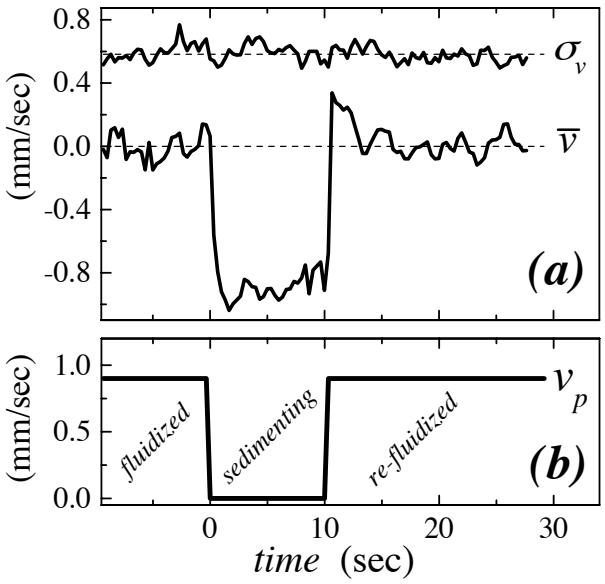

FIG. 15: Comparison of fluidization and sedimentation. (a) the velocity fluctuations σ_v and mean velocity $\overline{v}$ as a function of time t. (b) The upward fluid velocity v_p of the fluidized bed pump. For times $t < 0$, the pump is on, and the particles are stably fluidized. At time $t = 0$, the fluidization pump is turned off, and the particle sediment downwards until, at $t = 10$ s, the pump is turned back on to re-fluidize the system. The fluctuation magnitudes σ_v show no discernible difference between fluidization and sedimentation.

For a direct comparison on a typical sample, we show in Fig. 15 results for particle velocity fluctuations for the same sample in both fluidized and sedimenting states. Fluidization occurs for times leading up to $t = 0$ sec, when the fluid pump is on, and the average particle velocities in the vertical direction $\overline{v}$ are very close to zero. Sedimentation begins at $t = 0$ sec., when the fluid pump is temporarily turned off, and the particles move downwards with an average velocity $v_z \sim -0.9$ mm/s. (The rapid response of the particles to the turning on and off of the fluid pump reflects the lack of particle inertia.) Finally, at $t = 10$ s, after the particles have fallen ~ 1 cm (much less than the initial bed height $H \sim 18$ cm), the fluidizing pump is turned back on, and the particles are re-fluidized.

The remarkable feature seen in Fig. 15 is that the fluctuation magnitudes σ_v show no discernible difference throughout the transition from fluidization to sedimentation and back to fluidization. We interpret this as evidence that the particle fluctuation dynamics during fluidization and sedimentation are very similar. To examine this further, in the following two subsections we compare our fluidization results for ξ and σ_v to published results for the same quantities measured in sedimentation experiments.

1. Comparison to ξ from Sedimentation Experiments

Results for the correlation lengths ξ/a in sedimenting samples, covering a wide range of volume fractions $0.0001 \leq \phi \leq 0.50$, have been published by Segrè et *al.*[7,8]. The methodology by which ξ was measured differs from that used here during fluidization. In the sedimentation experiments, because of the limited time during which the particle column is falling, it was not possible to measure the fluctuations at different heights. Rather, a fixed camera recorded data continuously while the column fell past. This produced a single value of ξ that represents correlation values *averaged* over a large portion of the column, $0.25 \lesssim z/H \lesssim 0.75$. When results from samples of various average concentrations ϕ_0 were collected, the data were consistent with the scaling relation $\xi_S = 11a\phi_0^{-1/3}$.[7,8] For a meaningful comparison to our fluidization results, we thus need to first perform a similar height-averaging procedure to our data from Fig. 14, i.e. $\langle\xi(z)\rangle \simeq \frac{2}{H}\int_{0.25H}^{0.75H}\xi(z)dz$, with results plotted in the form $\langle\xi(z)\rangle$ vs. a in the inset of Fig. 16. The data fit well to $\langle\xi(z)\rangle \approx (25.8 \pm 2)a$, in remarkably good agreement with the scaling relation from sedimentation, $\xi_S = 11a\phi_0^{-1/3} = 23.7a$.

We emphasize again that the scaling relation found in sedimentation, $\xi_S = 11a\phi_0^{-1/3}$, represented a single, height-averaged, correlation length for a column of mean concentration ϕ_0. By comparison, our fluidization results in Figs. 9 and 14 display the complete height dependence of both ξ and ϕ from *within* a single column. By combining these data, we can ask a new question. Can the scaling form $\xi = 11a\phi^{-1/3}$ be used to predict the local values of ξ from the local values of ϕ *within* a single column? To answer this, we plot in Fig. 16 results from all four fluidized beds for $\xi(z)/a$ vs. the corresponding local volume fractions $\phi(z)$. It is immediately apparent that the scaling form does not describe the data, and has the opposite dependence on ϕ. Moreover the data points themselves do not collapse together, suggesting that, unlike the column averaged values $\langle\xi(z)\rangle$, the values of ξ within a column are not a unique function of ϕ alone.

2. Comparison to σ_v from Sedimentation Experiments.

Results for the velocity fluctuations σ_v in semi-dilute sedimenting samples have been published by numerous groups. Guazzelli[24] was the first, and found for a sample at the same concentration used here, $\phi_0 = 0.10$, that $\sigma_v/v_{sed} = 0.97 \pm 0.19$. Later, Segrè[8] measured $\sigma_v/v_{sed} = 0.70 \pm 0.08$ at $\phi = 0.05$, and $\sigma_v/v_{sed} = 0.9 \pm 0.1$ at $\phi = 0.13$. All of these values reflect height-averaged values of the falling columns, as described above. Ladd et al.[15] also conducted Lattice Boltzmann simulations of up to $32,000$ particles sedimenting in a fully bounded box at $\phi_0 = 0.13$. They found $\sigma_v/v_{sed} \simeq 0.6$ for the largest systems. All of these sedimentation values are in reasonably good

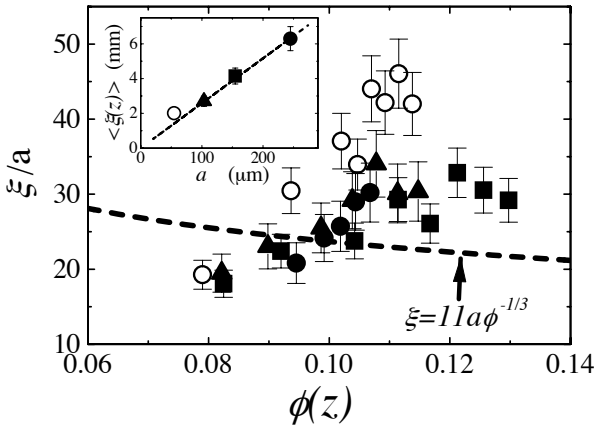

FIG. 16: Inset: Height averaged values $\overline{\xi}(z)$ vs. particle size a. The dashed line is a fit to $\overline{\xi} = 12a\phi_0^{-1/3}$. Main figure: velocity correlation lengths ξ/a vs. volume fraction ϕ. The dashed line represents the sedimentation scaling equation, $\overline{\xi} = 11a\phi_0^{-1/3}$, for the height averaged correlation lengths[7].

agreement with our fluidization results shown in Fig. 13, where near to the middle of the columns, $0.6 \lesssim \sigma_v/v_p \lesssim 0.9$.

IV. EVALUATION OF THE MUCHA AND BRENNER STRATIFICATION MODEL

The main aim of section III is to describe results for the particle dynamics during stable fluidization of a variety of different sized particle beds. We are not aware of other published results or predictions, either experimental or theoretical, for the specific forms of the quantities we measured, $\phi(z)$, $\nabla\phi(z)$, $\sigma_v(z)$ or $\xi(z)$, in similar fluidized beds. Published results are available for some of these properties in similar systems that are not fluidized, but rather are sedimenting downwards. Significantly, we were able to make a connection between fluidization and sedimentation by showing in Fig. 15 that the local velocity fluctuations in a typical sample are very similar in either mode. A subsequent comparison confirms this connection by showing that our average correlation lengths $\langle\xi(z)\rangle$ and velocity fluctuations σ_v in fluidized beds agree quite well with published results in sedimenting systems. Building upon this link, and in the absence of relevant fluidization theories, we therefore find it worthwhile to turn to theories of particle sedimentation to help explain our data.

The Mucha and Brenner model[12,13], as outlined in the introduction, is a recent theory of sedimentation that argues that the value of the local velocity correlation lengths ξ are primarily determined by the local degree of stratification $\nabla\phi$, see Eq. (1). Results in support of this model, from numerical simulations[12], have been confined to the transition region near the top particle interface, but whether it can provide a complete description of ξ over the entire sedimenting column remains an open question. The importance of the MB model, if verified, is that it would provide a new insight into the origin of the heretofore poorly understood fundamental lengthscale ξ that is ubiquitously seen in both fluidized and sedimenting systems.

For a complete test of the MB model, in each of the four beds we input fits to our data for $\phi(z)$ and $\nabla\phi(z)$ into Eq. (1) to generate model predictions for the velocity correlation lengths $l(z)/a$. These values are then directly compared to our correlation measurements $\xi(z)/a$. Figure 14 shows the results. The solid lines are the MB model predictions, and the symbols our data. Significantly, there is very good agreement between theory and experiment for all four fluidized beds. The adjustable fit constant c_0, which is not specified by the theory but is expected to be of order 1, has a single value, $c_0 = 0.82$, for the 3 scaling samples, $a \gg a^*$. For the non-scaling sample, with $a \sim a^*$, the model similarly works well, but requires a slightly lower fit value, $c_0 = 0.70$. The agreement is all the more impressive given that the gradients $\nabla\phi(z)$ are highly non-linear, strongly varying, functions of height z. The model Eq. (1) can also be simplified further by noting that the term $[\phi S(\phi)]^{1/5}$ is nearly constant over a wide range of volume fractions, $[\phi S(\phi)]^{1/5} = 0.52 \pm 0.03$ for $0.04 \leq \phi \leq 0.30$. In the scaling regime, $a \gg a^*$, therefore

$$\xi(z)/a \approx 0.43[-a\nabla\phi(z)]^{-2/5}. \qquad (2)$$

The truly remarkable feature about the MB model is that it accounts for the characteristic length scale of the velocity fluctuations, ξ, from which the magnitudes of the velocity fluctuations and diffusion coefficients can be calculated[7,8], *solely* from measurements of the stationary concentration profiles $\phi(z)$. Its validity corroborates the basic assumption of the model, that the velocity fluctuations are controlled by the concentration stratification $\nabla\phi$.

A. Re-derivation of the MB Model

Finally, we show that the MB model Eq. (1), obtained by Mucha and Brenner on the basis of physical arguments concerning buoyancy matching, can also be derived from a general advection-diffusion model of steady state sedimentation. In this model, as originally proposed by Kynch[25], the local particle concentration varies in time as

$$\partial\phi/\partial t = \nabla[\phi v + D\nabla\phi]. \qquad (3)$$

In our experiments, we achieve stable fluidization so that, when averaged over the short fluctuation lifetimes τ ($\sim \xi/\sigma_v \sim 5-10$ s), the concentration profiles $\phi(z)$ shown in Fig. 9 are *time-independent* quantities. Expressed mathematically, $\partial\langle\phi\rangle_\tau/\partial t = 0$, where $\langle\cdots\rangle_\tau$ represents an average over times greater than τ. For a stably

fluidized system, Eq. (3) predicts that the time averaged advective, $J_A = \langle \phi v \rangle_\tau$, and diffusive, $J_D = -\langle D \nabla \phi \rangle_\tau$, terms are equal at all positions in the particle column.

To evaluate the advective term, we expand to first order, $\phi(z,t) = \phi(z) + \delta\phi(z,t)$, and $v(z,t) = \langle v(z,t) \rangle_\tau + \delta v(z,t)$. (For compactness, we will simplify the notation below by not writing the explicit z dependence, i.e. $\phi(z) \to \phi$, but all quantities in general depend upon z). Since the mean particle velocity in a fluidized bed vanishes, $\langle v \rangle_\tau = 0$, and the time averaged fluctuations are zero, $\langle \delta\phi \rangle_\tau = 0$ and $\langle \delta v \rangle_\tau = 0$, the advective term reduces to $J_A = \langle \delta\phi \delta v \rangle_\tau$, which is non zero because velocity and concentration fluctuations are anti-correlated (denser regions fall, lighter regions rise)[1,9]. If we approximate the fluctuation terms by their *rms* values, i.e. $\delta\phi \sim \sigma_\phi = \sqrt{\langle (\delta\phi)^2 \rangle_\tau}$, then

$$J_A \approx -\sigma_\phi \sigma_v. \tag{4}$$

To evaluate the diffusive term, J_D, we use the published result (from sedimentation experiments[8,24]) that the hydrodynamically induced particle diffusion coefficient is related to the fluctuations through $D \approx \sigma_v \xi$, so that

$$J_D \approx -\sigma_v \xi \nabla \phi. \tag{5}$$

For the stability criteria, $J_A = J_D$, the velocity terms σ_v cancel out, leaving the simple relation $\nabla\phi = -\sigma_\phi/\xi$, that relates the stratification to the concentration fluctuations. To evaluate σ_ϕ, we use the same Poisson model as Mucha and Brenner, $\sigma_\phi = \sqrt{\phi S(\phi) a^3/\xi^3}$. Here, $S(\phi)$ is the structure factor of random hard spheres needed at moderate to high concentrations to account for excluded volume effects[8]. Finally, we solve for the correlation length ξ and obtain

$$\xi/a = c_0 [\phi S(\phi)]^{1/5} [-a \nabla \phi]^{-2/5}, \tag{6}$$

which is identical to the MB model Eq. (1).

The new insight provided by this re-derivation of the MB model is that it explicitly shows that Eq. (1) is contingent upon *steady state* behavior, in which $\partial \langle \phi \rangle_\tau / \partial t = 0$. This highlights the advantage of testing this model in fluidized beds, which produce time invariant concentration profiles. In sedimentation on the other hand, several studies have reported that the concentration profile continues to evolve as the column is falling[10,16,17]. Consequently, the profile may or may not reach a steady state before the column collapses to the bottom. This derivation explicitly shows that in columns with time varying concentration profiles, i.e. $\partial\phi(z,t)/\partial t \neq 0$, the advective and diffusive particle flux terms would not be balanced, and the MB model Eq. (1) would not hold true.

V. DISCUSSION AND CONCLUSIONS

In this article we present results on the particle dynamics in liquid fluidized beds at low Reynolds number. Our primary aim is to examine the behavior of the fluctuating particle velocities and the stationary concentration profiles. We chose to do this in moderately concentrated samples, all of mean concentration $\phi_0 = 0.10$. To examine how the velocity and concentration profiles depend upon system size, we used a single cell geometry, but varied the particle size a by a factor of ~ 4.5 so that the system size N varies by almost two orders of magnitude.

For all particle sizes, the measured concentration gradients $\nabla\phi$, fluctuation magnitudes σ_v, and correlation lengths ξ, all display $z-$dependent profiles in the particle columns. These profiles are found to change in magnitude, but not form, when the particle sizes a are varied over a wide range. Specifically, we find a scaling regime for particles larger than a critical size, $a \gg a^*$, in which the data profiles from different particle sizes collapse together when plotted in the forms $-a\nabla\phi(z)$, $\xi(z)/a$, and $\sigma_v(z)/v_p$. (see Figs. 12(b), 13, and 14). These simple scalings with particle size demonstrate the universality of the particle dynamics and structure in fluidization.

The new scalings also quantify how the bed properties depend upon system size. In our experiments, the number of particles fluidized, $N = TWH\phi_0/(4/3)\pi a^3 \propto 1/a^3$, increases with decreasing particle size. The scaling region is found when $a \gg a^*$, or equivalently $N \ll N^*$, where $N^* \approx 35$ million particles. In this regime, the stratification scaling of $a\nabla\phi(z)$ can similarly be written as a $N^{-1/3}\nabla\phi(z)$ scaling, explicitly showing that the concentration gradient grows with N. Interestingly, in the limit of very small systems, the gradients vanish, i.e. $\lim_{N\to 0} \nabla\phi(z) = 0$, resulting in what would be a uniformly concentrated particle bed. This is an important point that shows that it would generally be easier to observe concentration gradients in experiments, as opposed to simulations, since experimental system sizes are usually much larger. On the other hand, Ladd[15] simulated the sedimentation of ~ 32000 particles (in a square cell geometry) at $\phi_0 = 0.13$ and, while looking across the middle of the column, found evidence for an extremely small gradient $-a\nabla\phi$ "*of order* 10^{-5}". This result agrees well with our measurements shown in Fig. 12, where near mid-height, $-a\nabla\phi \approx 2 - 3 \cdot 10^{-5}$.

Evidence is also presented that the particle dynamics in fluidized beds can be closely connected to that seen in similar systems that are sedimenting downwards. We first demonstrate this for a typical sample in Fig. 15, where the magnitude of the velocity fluctuations show no discernible difference between the two modes. To pursue this further, we apply the same column averaging methods to our data that has been used in sedimentation experiments to extract a single value for σ_v and ξ in each of our fluidized beds. These values were found to be in good agreement with published findings in sedimentation, further connecting the two. It is known, however, that clear differences do exist between fluidization and sedimentation, particulary regarding whether or not the systems are in a steady state. Numerous studies[10,17,26] beginning with Guazzelli[16], have shown that the particle

dynamics (σ_v, ξ, $\nabla\phi\ldots$) in sedimentation can be strongly time-dependent as the particles fall, in which case a steady state is not achieved. In fluidized systems, on the other hand, as the column stays suspended indefinitely, a steady state is eventually reached, as we find here. We note that in our fluidization/sedimentation comparisons, we compared to sedimentation data thought to be in near steady state conditions.

A further, and central, finding in this paper is the verification in Sec. IV of the Mucha and Brenner model for the velocity correlation lengths $\xi(z)$. The model predicts that $\xi(z)$ can be calculated solely from the concentration profile $\phi(z)$ (and its derivative $\nabla\phi(z)$). We measured $\phi(z)$, and found that the MB model predictions for $\xi(z)$ from Eq. (1) were in very good agreement with our correlation length measurements in all four beds, and at all heights within each bed. The physical argument used by Mucha and Brenner is that, owing to buoyancy forces, concentration gradients limit the maximal size over which particle velocities can be correlated, and this leads to the relation between ξ and $\nabla\phi$ given in Eq. (1). In sec. IV A, we also show an alternative derivation of Eq. (1), starting from a general advection-diffusion equation. The physical picture we used is seemingly different from the MB line of reasoning, yet both yield the same relation between ξ and $\nabla\phi$. In our derivation, when the system is in a steady state, i.e. $\partial\langle\phi(z,t)\rangle_\tau/\partial t = 0$, the diffusive flux generated by concentration gradients, $D\nabla\phi$, is counterbalanced by an advective flux due to the fluctuations, $\sigma_\phi\sigma_v$, which leads to Eq. (1).

Several key questions still remain to be answered, starting with the observation that the MB relation Eq. (1) requires a knowledge of the stratification in $\nabla\phi$ for a determination of the correlation length ξ, but does not allow for an *a priori* calculation of either quantity. Additionally, while we found there to be an overall system size dependence for several properties in steady state sedimentation, we did not vary the different dimensions of the cell (TWH) independently, so it is not known whether some dimensions of the cell are more influential in this regard than others. Future experiments using different aspect ratio cells are being planned to help resolve these issues.

We thank Shang Tee and Tony Ladd for stressing the importance of using nearly monodisperse beads, and Alex Levine, Dave Weitz and Michael Brenner for many discussions. (corresponding author: psegre@physics.emory.edu)

[1] E.J. Hinch, in *Disorder in Mixing*, edited by E. Guyon *et al.*, Kluwer Academic, Dordrecht, 1988, p. 153.

[2] R.E. Caflisch and J.H.C. Luke, *Variance in the Sedimentation Speed of a Suspension*, Phys. Fluids **28**, 259 (1985).

[3] D.L. Koch and E.S.G. Shaqfeh, *Screening in Sedimenting Suspensions*, J. Fluid Mech. **224**, 275 (1991).

[4] A. Levine, S. Ramaswamy, E. Frey and R. Bruinsma, *Screened and Unscreened Phases in Sedimenting Suspensions*, Phys. Rev. Lett. **81**, 5944 (1998).

[5] P. Tong and B.J. Ackerson, *Analogies Between Colloidal Sedimentation and Turbulent Convection at High Prandtl Numbers*, Phys. Rev. E **58**, 6931 (1998).

[6] M.P. Brenner, *Screening Mechanisms in Sedimentation*, Phys. Fluids **11**, 754 (1999).

[7] P.N. Segrè, E. Herbolzheimer and P.M. Chaikin, *Long Range Correlations in Sedimentation*, Phys. Rev. Lett. **79**, 2574 (1997).

[8] P.N. Segrè, F. Liu, P. Umbanhower and D.A. Weitz, *An Effective Gravitational Temperature for Sedimentation*, Nature **409**, 594 (2001).

[9] X. Lei, B.J. Ackerson and P. Tong, *Settling Statistics of Hard Sphere Particles*, Phys. Rev. Lett. **86**, 3300 (2001).

[10] S.Y. Tee et *al.*, *Nonuniversal Velocity Fluctuations of Sedimenting Particles*, Phys. Rev. Lett. **89**, 054501 (2002).

[11] J.H.C. Luke, *Decay of Velocity Fluctuations in a Stably Stratified Suspension*, Phys. Fluids **12**, 1619 (2000).

[12] P.J. Mucha and M.P. Brenner, *Diffusivities and Front Propagation in Sedimentation*, Phys. Fluids **15**, 1305 (2003).

[13] P.J. Mucha et *al.*, *A Model for Velocity Fluctuations in Sedimentation*, J. Fluid Mech. **501**, 71 (2004).

[14] D. Saintillan, E.S.G. Shaqfeh and E. Darve, *The Effect of Stratification on the Wave Number Selection in the Instability of Sedimenting Spheroids*, Phys. Fluids **18**, 121503 (2006).

[15] A.J.C. Ladd, *Effects of Container Walls on the Velocity Fluctuations of Sedimenting Spheres*, Phys. Rev. Lett. **88**, 48301 (2002)

[16] E. Guazzelli, *Evolution of Particle-Velocity Correlations in Sedimentation*, Phys. Fluids **13**, 1537 (2001).

[17] S.L. Dance and M.R. Maxey, *Particle Density Stratification in Transient Sedimentation*, Phys. Rev. E **68**, 31403 (2003).

[18] J. Martin, N. Rakotomalala and D. Salin, *Hydrodynamic Dispersion of Noncolloidal Suspensions: Measurement from Einstein's Argument*, Phys. Rev. Lett. **74**, 1347 (1995).

[19] P.N. Segrè, *Origin of Stability in Sedimentation*, Phys. Rev. Lett. **89**, 254503 (2002).

[20] R.J. Adrian, *Particle-Imaging Techniques for Experimental Fluid Mechanics*, Annu. Rev. Fluid Mech. **23**, 261 (1991).

[21] L. Bergougnoux, S. Ghicini, E. Guazzelli and J. Hinch, *Spreading Fronts and Fluctuations in Sedimentation*, Phys. Fluids **15**, 1875 (2003).

[22] J.F. Richardson and W.N. Zaki, *Sedimentation and Fluidisation: Part* 1:, Trans. Inst. Chem. Eng. 32, 35 1954.

[23] N.-Q. Nguyen and A.J.C. Ladd., *Sedimentation of Hard-Sphere Suspensions at Low Reynolds Number*, J. Fluid Mech. **525**, 73 (2005).

[24] H. Nicolai and E. Guazzelli, *Effect of the Vessel Size on the Hydrodynamic Diffusion of Sedimenting Spheres*, Phys. Fluids **7**, 3 (1995). H. Nicolai et *al.*, *Particle Velocity Fluctuations and Hydrodynamic Self-Diffusion of Sedimenting Non-Brownian Spheres*, Phys. Fluids **7**, 12 (1995).

[25] G.J. Kynch, *A theory of sedimentation*, Trans. Faraday

Soc. **48** 166, (1952).
[26] E.S. Asmolov, *Evolution of Fluctuations in a Suspension Sedimenting in a Container Bounded by Horizontal Walls*, Phys. Fluids **16**, 3086 (2004).